Electrical Capacitance Tomography to monitor unsaturated moisture ingress in cement-based materials

Antti Voss[1], **Mohammad Pour-Ghaz**[2], **Marko Vauhkonen**[1], **Aku Seppänen**[1]

[1] Department of Applied Physics, University of Eastern Finland, Kuopio, FINLAND, antti.voss@uef.fi, marko.vauhkonen@uef.fi, aku.seppanen@uef.fi

[2] Deparment of Civil, Construction and Engineering, North Carolina State University, Raleigh, NC 27695, USA, mpourgh@ncsu.edu

Keywords: Non-destructive testing, Electrical Capacitance Tomography (ECT), Permittivity, Imaging, Moisture flow.

Abstract

This paper investigates the feasibility of electrical capacitance tomography (ECT) for monitoring unsaturated moisture flow in cement-based materials. In ECT, the electrical permittivity distribution within an object is reconstructed based on capacitive measurements made from the object's surface. In the experiments, mortar specimens with different w/c ratios (0.25, 0.45 & 0.60) were monitored with ECT during moisture ingress. The results demonstrate that ECT is able to image the moisture ingress within the specimens, and further, to distinguish between different moisture flow rates in mortars with different porosities resulting from differing w/c ratios. These findings suggest that ECT could provide a non-destructive tool for monitoring and visualizing the rate of moisture ingress in cement-based materials.

1. INTRODUCTION

The ability to impede water ingress is a feature of durable concrete because the durability of concrete largely depends on its mass transport properties [1]. Various methods exist for monitoring, visualizing and quantifying moisture ingress in cement-based materials, including neutron imaging [2, 3], gamma-ray [4], X-ray [4] and electrically-based methods [5, 6]. However, the existing methods have their own advantages and limitations, for example, gamma-ray, X-ray and neutron imaging have high spatial resolution, but they are commonly limited to small specimens and laboratory environment due to large attenuation. Electrically-based methods, in contrast, have a low spatial resolution, but they are inexpensive, easy and quick to perform.

Traditional electrically-based methods for the evaluation of the moisture flow rely on point measurements. For example, electrical impedance spectroscopy (EIS) [6, 7], and impedance measurements using a single frequency alternating current [7], have been used for monitoring unsaturated flow in cement-based materials. These techniques provide "some measure" of the water front location. They may also provide some rough information about the moisture distribution (for example, an approximate depth of a highly saturated region); but they do not provide a profile of the moisture distribution.

Electrical resistance tomography (ERT) is an imaging modality in which the spatially distributed electrical conductivity within an object is reconstructed on the basis of current injections and voltage measurements acquired from the object boundary. ERT has been shown to provide information on the distribution of moisture in cement-based materials [8–11]. ERT, however, has some limitations. In particular, ERT requires a good ohmic contact between the electrodes and the target surface. Thus ERT measurements on samples with a very low moisture content (i.e. high electrical resistivity) can be problematic [12].

While ERT and other methods based on resistance or impedance measurements suffer from the above limitations, capacitive measurements are suitable for dry concrete. Indeed, capacitive measurements do not require ohmic contact with the object. Moreover, capacitive measurements are sensitive to

the presence of moisture in concrete, because the permittivity contrast between dry and wet concrete is high – the relative permittivity of dry concrete is typically between 3 and 6, while the relative permittivity of water in room temperature is approximately 80. Capacitive surface sensors have been applied to determining the cover-zone moisture content [11] and to inspecting defects [13] in concrete. Thus far, however, capacitive measurements have not been used for tomographic imaging of concrete or other cement-based materials.

An imaging modality which uses inter-electrode capacitances measured from the object surface to reconstruct the electrical permittivity distribution inside the object is referred to as Electrical capacitance tomography (ECT). ECT has been used, for example, for estimating the moisture content in soil [14] and for monitoring mixing and drying of wet granules [15]. In this paper, the feasibility of ECT for imaging cement-based materials is studied. Especially, we investigate whether ECT could provide information on moisture distributions in cement-based materials. ECT is tested with a set of experiments where unsaturated water ingress in mortar is induced. Mortars with different porosities are used, to study the ability of ECT to distinguish between different flow rates.

2. ELECTRICAL CAPACITANCE TOMOGRAPHY

In electrical capacitance tomography (ECT), the electrical capacitances between electrodes placed around the periphery of an object are measured (see Fig. 1). Based on these measurements, the electrical permittivity distribution $\varepsilon(\boldsymbol{x})$ inside the object is reconstructed. Here, $\boldsymbol{x} \in \Omega$ denotes the spatial coordinate within the target volume Ω. The permittivity distribution can be expressed as $\varepsilon(\boldsymbol{x}) = \varepsilon_{\text{vac}}\varepsilon_r(\boldsymbol{x})$, where ε_{vac} is the vacuum permittivity ($\varepsilon_{\text{vac}} \approx 8.8542$ x 10^{-12} Fm^{-1}), and $\varepsilon_r(\boldsymbol{x}) \geq 1$ is the relative permittivity of the material.

A typical measurement strategy is to excite one electrode at a time to some fixed potential U, while the others are grounded. Inter-electrode capacitances $C_{i,j}$ are measured between the excited and grounded electrodes; with L electrodes $m = \frac{L(L-1)}{2}$ measurements are obtained. Fig. 1 illustrates the measurement protocol for two different excitations.

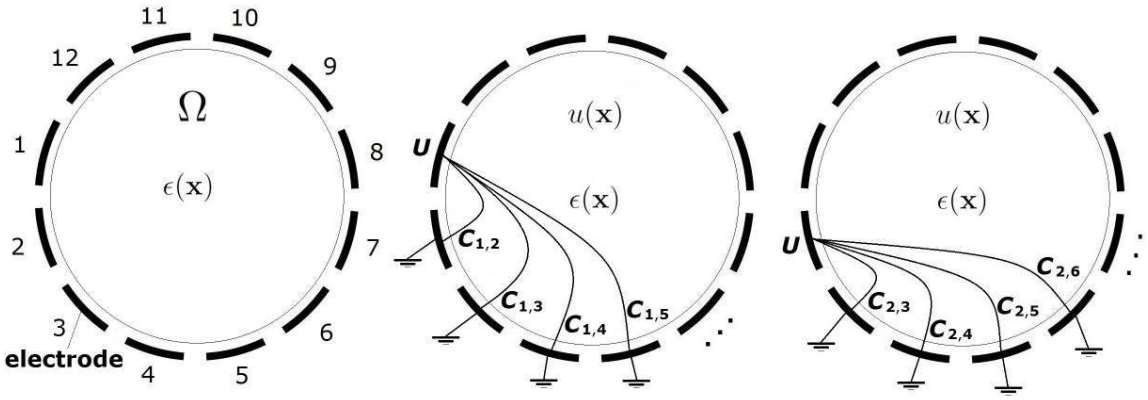

Figure 1 : Left: Illustration of an ECT experiment. Middle and right: Capacitance measurements corresponding to two potential excitations.

A mathematical model that connects the inter-electrode capacitances $C_{i,j}$ with the spatially distributed permittivity $\varepsilon(\boldsymbol{x})$ and electric potential $u(\boldsymbol{x})$ consists of Poisson equation

$$\nabla \cdot \varepsilon(\boldsymbol{x}) \nabla u(\boldsymbol{x}) = 0, \quad \boldsymbol{x} \in \Omega \tag{1}$$

and suitable boundary conditions that depend on the measurement set-up (see for example [15]). Equation (1) can be derived from Maxwell's equations by assuming static electrical conditions (electrostatic approximation) and ignoring the conductive properties of the medium ($\sigma(\boldsymbol{x}) \approx 0$, where $\sigma(\boldsymbol{x})$ is the

electrical conductivity). The electrical capacitance $C_{i,j}$ between the ith and jth electrode depends on the permittivity and electric potential as follows

$$C_{i,j}(\varepsilon) = \frac{1}{V_{i,j}} \int_{e_j} \varepsilon(\mathbf{x}) \frac{\partial u(\mathbf{x})}{\partial \mathbf{n}} dS, \tag{2}$$

where $V_{i,j}$ is the potential difference between the ith and jth electrode, e_j denotes the surface of the jth electrode, and $\partial u(\mathbf{x})/\partial \mathbf{n}$ is the derivative of the potential in the direction of the outward unit normal vector $\mathbf{n}$.

The above forward model is usually approximated by finite element method (FEM), leading to a form $C_{i,j} = h_{i,j}(\boldsymbol{\varepsilon_r})$, where $\boldsymbol{\varepsilon_r}$ is a finite dimensional representation of the relative permittivity distribution $\varepsilon_r(\boldsymbol{x})$, and $h_{i,j}(\boldsymbol{\varepsilon_r})$ is a mapping resulting from the finite element (FE) approximation (for details of the FE approximation, see e.g. [16]). By stacking the models corresponding to a set of m capacitance measurements to a vector, and by assuming additive measurement noise, the observation model of ECT can be written in the form

$$\boldsymbol{C} \quad = \quad \boldsymbol{h}(\boldsymbol{\varepsilon_r}) + \boldsymbol{v}_c, \tag{3}$$

where $\boldsymbol{C} = [C_1, \ldots, C_m]^T$ is a vector that contains the measured capacitances, vector $\boldsymbol{v}_c$ consists of the corresponding measurement noises, $\boldsymbol{v}_c = [v_1^c, \ldots, v_m^c]^T$, and $\boldsymbol{h}(\boldsymbol{\varepsilon_r}) = [h_{1,2}(\boldsymbol{\varepsilon_r}), \ldots, h_{L-1,L}(\boldsymbol{\varepsilon_r})]^T$ is the concatenated model.

In this paper, the inverse problem i.e. the estimation of the permittivity distribution is solved using so-called difference imaging approach. In ECT difference imaging, the change of the time-varying permittivity is estimated on the basis of the difference in ECT data before ($\boldsymbol{C}_{\text{ref}}$) and after the change ($\boldsymbol{C}$) [17]. In linearized difference imaging, the observation model (3) for $\boldsymbol{C}_{\text{ref}}$ and $\boldsymbol{C}$ is approximated by first order Taylor polynomial. Then substracting the linearized models, a linear observation model for the difference data $\Delta\boldsymbol{C} = \boldsymbol{C} - \boldsymbol{C}_{\text{ref}}$ can be written as

$$\Delta\boldsymbol{C} \quad = \quad \boldsymbol{J}\Delta\boldsymbol{\varepsilon_r} + \Delta\boldsymbol{v}_c \tag{4}$$

where $\Delta\boldsymbol{\varepsilon_r} = \boldsymbol{\varepsilon_r} - \boldsymbol{\varepsilon}_{\boldsymbol{r},\text{ref}}$ is the permittivity difference, $\Delta\boldsymbol{v}_c = [(v_1^c - v_1^{c,\text{ref}}), ..., (v_m^c - v_m^{c,\text{ref}})]^{\text{T}}$ is the difference of the noise terms and $\boldsymbol{J}$ is the Jacobian matrix computed at a chosen linearization point. An estimate $\widehat{\Delta\boldsymbol{\varepsilon_r}}$ for the change of the relative permittivity is calculated as a Tikhonov regularized [18] solution based on the linearized observation model (4)

$$\widehat{\Delta\boldsymbol{\varepsilon_r}} = \arg\min_{\Delta\boldsymbol{\varepsilon_r}} \{ \|L_{\Delta\boldsymbol{v}_c}(\Delta\boldsymbol{C} - \boldsymbol{J}\Delta\boldsymbol{\varepsilon_r})\|^2 + \|L_{\Delta\boldsymbol{\varepsilon_r}}\Delta\boldsymbol{\varepsilon_r}\|^2 \}, \tag{5}$$

where $L_{\Delta\boldsymbol{v}_c}$ is the weighting matrix, defined as $L_{\Delta\boldsymbol{v}_c}^T L_{\Delta\boldsymbol{v}_c} = \Gamma_{\Delta\boldsymbol{v}_c}^{-1}$, where $\Gamma_{\Delta\boldsymbol{v}_c}$ is the covariance of the measurement noise term $\Delta\boldsymbol{v}_c$, and $L_{\Delta\boldsymbol{\varepsilon_r}}$ is a smoothness promoting regularization matrix. For the construction of $L_{\Delta\boldsymbol{\varepsilon_r}}$, see [19].

The global linearization of the non-linear observation model (3) made in difference imaging can lead to qualitative results, if the linearization point is poorly chosen or the changes in the target permittivity are large. On the other hand, difference reconstruction method is relatively robust and can tolerate modeling errors, and it is also fast to compute.

Note that when monitoring moisture ingress with ECT, the above approximation of conductive effects being negligible is one of the sources of modeling errors. Because the electrical conductivity of mortar increases when the moisture content increases, the error caused by this approximation does not entirely cancel out in the subtraction $\boldsymbol{C} - \boldsymbol{C}_{\text{ref}}$. Nevertheless, the approximation can still be adequate for (at least) qualitative imaging of moisture flow with ECT, and is used in this paper.

3. EXPERIMENTS

3.1 General

In the experiments, water infiltrated into cylindrical mortar specimens of three different w/c ratios: 0.25, 0.45 and 0.60. The experimental setup is schematically illustrated in Figure 2. A reservoir attached on top of each specimen was filled with water in the beginning of the experiment. ECT measurements were carried out sequentially during the water infiltration. More detailed explanation of the experiments can be found from the article [20].

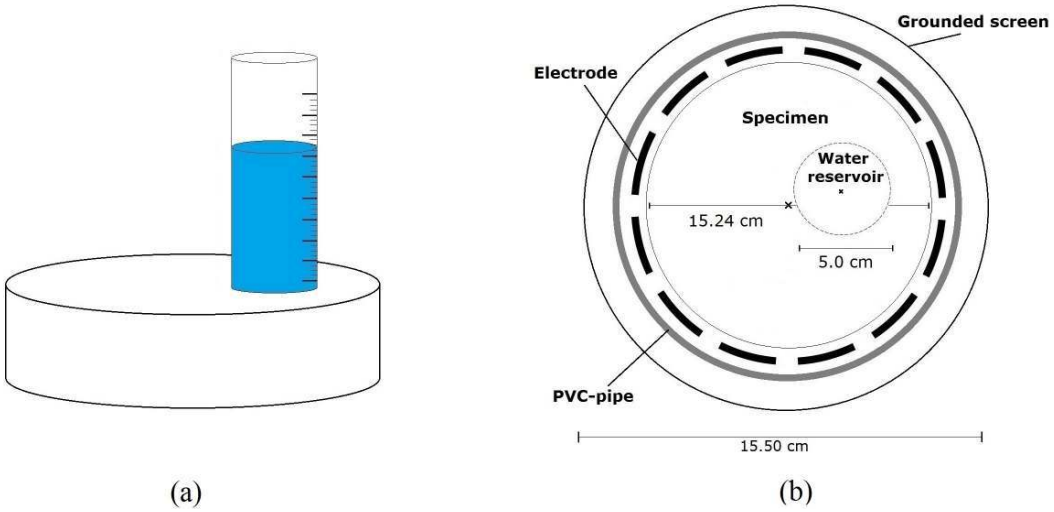

Figure 2 : (a) Schematic illustration of a specimen and a water reservoir. (b) Schematic top-view illustration of the ECT setup and specimen (not to scale).

3.2 Water infiltration

A portion of a graduated cylinder was used as a water reservoir. Fig. 2 schematically illustrates the location and size of the water reservoir. The top surfaces of the specimens around the water reservoirs were sealed with transparent tape to avoid evaporation. The water reservoir was filled with de-ionized water at the beginning of the experiment. To measure the amount of absorbed water, a photograph of the graduated cylinder was taken every hour using a digital camera. Using these photographs, the volume of absorbed water as a function of time was determined. The duration of each experiment was adjusted based on the rate of absorption in the corresponding specimen. The water ingress continued 14, 6 and 3 days for the specimens with w/c of 0.25, 0.45 and 0.60, respectively.

3.3 ECT monitoring during water infiltration

The experimental setup is shown in Fig. 3(b). Inter-electrode capacitances were measured using PTL300E (Process Tomography Ltd.) electrical capacitance tomography system (see for more details of the system in [21]). The ECT fixture used in this study consisted of 12 copper electrodes, a PVC-pipe and an external metal screen (Figs. 2(b) and 3(a)). The electrodes were mounted on the inside wall of the PVC-pipe that was surrounded by the external electrically grounded screen. The screen was used for preventing the interference of external noise. The size of each electrode was 50 x 40 mm, and adjacent electrodes were separated by 3 mm wide electrically grounded axial guards.

In all experiments the electrodes covered the entire thickness of the specimen, and therefore, the capacitance measurements did not carry information on the variations of the permittivity in the vertical

direction (i.e., through the thickness of the sample). In other words, this kind of measurement setting only allowed 2D ECT imaging. ECT, however, is not limited to 2D imaging; 3D ECT is used in many applications, see e.g. [22, 23].

The measurement protocol described in Section 2 resulted in a total of 66 capacitance measurements. For all the specimens, the first set of ECT measurements was carried out before water was added to the reservoir. These data sets were used as reference measurements $\boldsymbol{C}_{\text{ref}}$ in difference imaging (see Section 2). After water addition, ECT measurements were continuously performed at a rate of 1 measurement frame per second throughout the experiment on each specimen until the water infiltration was stopped.

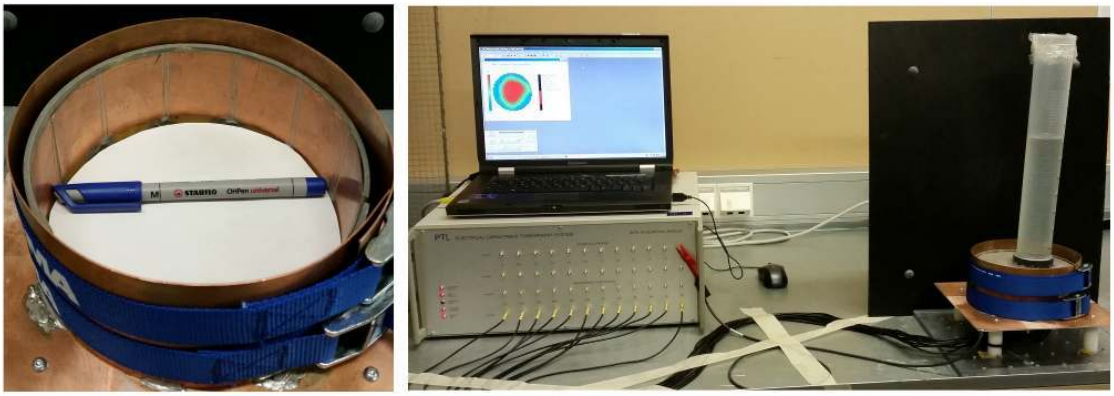

(a) (b)

Figure 3 : (a) An empty ECT measurement fixture. (b) PTL300E measurement system, and the experimental setup.

4. RESULTS AND DISCUSSION

The visually monitored water volumes (V_{w}) absorbed to the mortar specimens with different w/c ratios are shown in Fig. 4. As expected, the graphs indicate clear differences in the rates of absorption between the specimens. The specimen with highest w/c (0.60) has the highest absorption rate: in three days, approximately 140 ml of water is absorbed. The material with w/c ratio 0.45 has the second largest absorption rate, for this specimen it takes about 4.5 days to absorb the water volume of 140 ml. For the material with lowest w/c ratio (0.25), the absorption rate is very slow: only about 25 ml of water is absorbed in 14 days.

The images of the relative permittivity change $\Delta\varepsilon_r$ reconstructed with ECT are shown in Fig. 5. The figure shows the ECT reconstructions of all three specimens with different w/c ratios at times 8 h, 24 h, 48 h, 72 h, 6 days and 14 days. Note that ECT reconstructions of all specimens are not available corresponding to last two time instants.

All ECT images in Fig. 5 are presented in the same color scale to ease the comparison of the results between specimens. Black color in the ECT reconstructions denotes large positive change of $\Delta\varepsilon_r$ which indicates a high increase in the water content. Respectively, white color denoting a small negative permittivity change indicates a slight decrease in the water content. The change of the permittivity with respect to the initial state is expected to be non-negative in an experiment where water ingresses to porous medium. Hence the occurrences of the negative permittivity change in the ECT images are most likely reconstruction artefacts.

Fig. 5 shows the temporal evolutions of the permittivity change for all three specimens. In all cases, as the time evolves, the permittivity increases at the area that corresponds to the location of the water reservoir. Furthermore, although the ECT reconstructions are mostly qualitative, they show clear differences between permittivity changes corresponding to three different w/c ratios. Indeed, the ECT

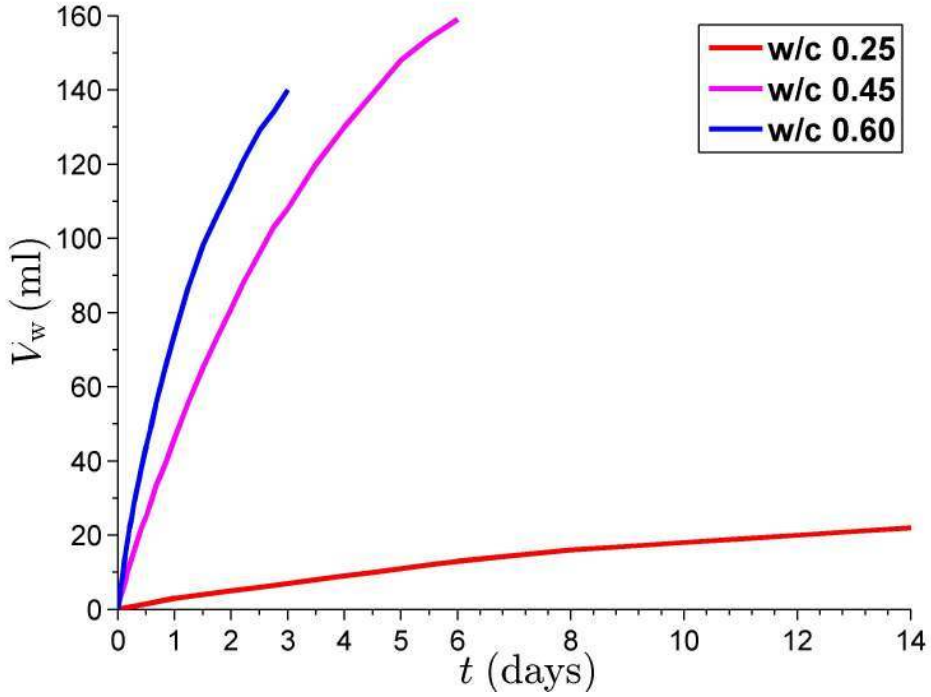

Figure 4 : The absorbed water volume V_w as functions of time for the mortar specimens with w/c ratios 0.60 (blue), 0.45 (purple) and 0.25 (red).

images show the most rapid increase of the permittivity in the most porous material (w/c ratio 0.60), where the water absorption was highest (cf. Fig. 4). The specimen with the lowest w/c ratio (0.25), where the absorption rate was slowest, shows also the slowest permittivity increase.

It is worth noting, that in this paper the reconstruction of the relative electrical permittivity distribution $\Delta\boldsymbol{\varepsilon_r}(x,t)$ was based on several approximations, including the linear approximation of the observation model, as well as neglecting the electrical conductivity change due to the absorption of water and the 3D effects of the moisture flow. On the other hand, it is promising that ECT responds consistently to the absorbed water volume despite the above approximations. The results suggest that ECT is able to detect the moisture ingress and distinguish between different water flow rates in cement-based materials.

5. CONCLUSIONS

In this paper, the feasibility of electrical capacitance tomography (ECT) for monitoring unsaturated moisture flow within cement-based materials was studied. To investigate the ability of ECT to distinguish between different flow rates, mortar specimens with three different w/c ratios (0.25, 0.45 and 0.60) were imaged during water ingress.

ECT was able to detect the evolution of moisture in all the specimens. The ECT reconstructions showed increasing permittivity during the moisture ingress, and the location of the area with the increased relative permittivity corresponded to the location of the water reservoir on top of the specimens. Furthermore, ECT showed clear differences between specimens with different w/c ratios; featuring the most rapid increase of the permittivity in the most porous material (w/c ratio 0.6) and the slowest increase of the permittivity in the material with the lowest porosity (w/c ratio 0.25).

The results of this paper demonstrate the feasibility of ECT for monitoring unsaturated moisture flow in cement based materials, and show that ECT is able to distinguish between different water flow rates. In the future, ECT might serve as a non-destructive tool for monitoring and visualizing the rate of

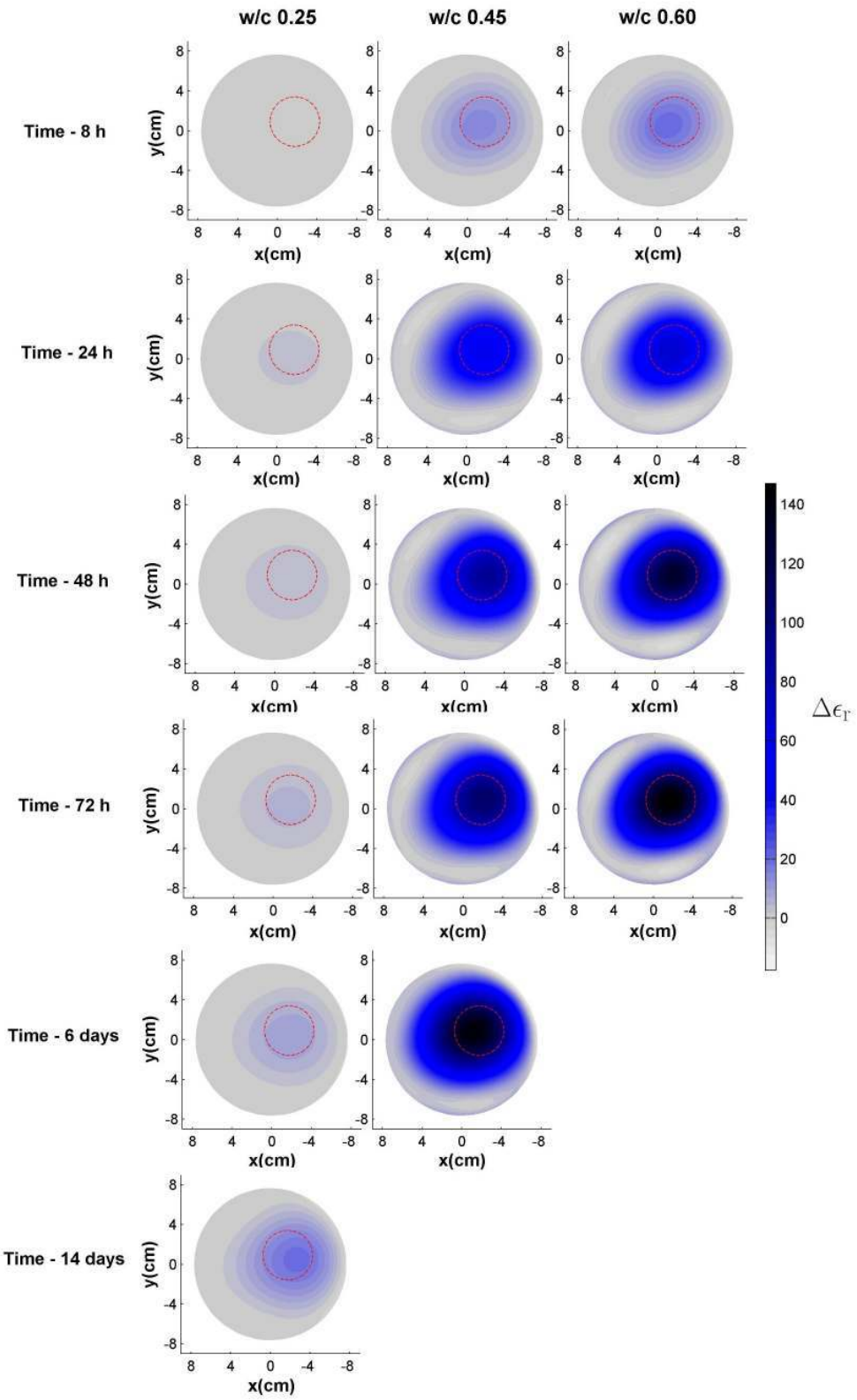

Figure 5 : The evolutions of the relative permittivity change reconstructed based on ECT. The columns from left to right correspond to w/c ratios 0.25, 0.45 and 0.60. The times of the ECT measurements are shown on the left side of each row. The dashed red circle indicates the location of the water reservoir.

moisture ingress in cement-based materials, and in turn, to provide information on the durability of the material.

REFERENCES

[1] Paulo J. M. Monteiro and P. Kumar Mehta. *Concrete Microstructure, Properties and Materials*. McGraw-Hill, 3 edition, 2006.

[2] H Pleinert, H Sadouki, and FH Wittmann. Determination of moisture distributions in porous building materials by neutron transmission analysis. *Materials and Structures*, 31(4):218–224, 1998.

[3] P Zhang, FH Wittmann, TJ Zhao, EH Lehmann, L Tian, and P Vontobel. Observation and quantification of water penetration into strain hardening cement-based composites (SHCC) with multiple cracks by means of neutron radiography. *Nuclear Instruments and Methods in Physics Research Section A: Accelerators, Spectrometers, Detectors and Associated Equipment*, 620(2):414–420, 2010.

[4] Staf Roels, Jan Carmeliet, Hugo Hens, Olaf Adan, Harold Brocken, Robert Cerny, Zbysek Pavlik, Armin T Ellis, Christopher Hall, Kumar Kumaran, et al. A comparison of different techniques to quantify moisture content profiles in porous building materials. *Journal of Thermal Envelope and Building Science*, 27(4):261–276, 2004.

[5] WJ McCarter, M Emerson, and H Ezirim. Properties of concrete in the cover zone: developments in monitoring techniques. *Magazine of Concrete Research*, 47(172):243–251, 1995.

[6] Farshad Rajabipour, Jason Weiss, John D Shane, Thomas O Mason, and Surendra P Shah. Procedure to interpret electrical conductivity measurements in cover concrete during rewetting. *Journal of materials in civil engineering*, 17(5):586–594, 2005.

[7] William J McCarter. Monitoring the influence of water and ionic ingress on cover-zone concrete subjected to repeated absorption. *Cement, Concrete and Aggregates*, 18(1), 1996.

[8] Milad Hallaji, Aku Seppänen, and Mohammad Pour-Ghaz. Electrical resistance tomography to monitor unsaturated moisture flow in cementitious materials. *Cement and Concrete Research*, 69:10–18, 2015.

[9] Danny Smyl, Milad Hallaji, Aku Seppänen, and Mohammad Pour-Ghaz. Three-dimensional electrical impedance tomography to monitor unsaturated moisture ingress in cement-based materials. *Submitted to Transport in Porous Media*.

[10] M. Buettner, A. Ramirez, and W. Daily. Electrical resistance tomography for imaging concrete structures. in: Structural materials technology an NDT Conference, San Diego, California, 1996.

[11] R. du Plooy, G. Villain, S. Palma Lopes, A. Ihamouten, X. Dérobert, and B. Thauvin. Electromagnetic non-destructive evaluation techniques for the monitoring of water and chloride ingress into concrete: a comparative study. *Materials and Structures*, pages 1–18, 2013.

[12] Kimmo Karhunen, Aku Seppänen, Anssi Lehikoinen, Paulo JM Monteiro, and Jari P Kaipio. Electrical resistance tomography imaging of concrete. *Cement and Concrete Research*, 40(1):137–145, 2010.

[13] Xiaokang Yin, DA Hutchins, GG Diamond, and P Purnell. Non-destructive evaluation of concrete using a capacitive imaging technique: Preliminary modelling and experiments. *Cement and Concrete Research*, 40(12):1734–1743, 2010.

[14] Nurzharina Binti Abd Karim and Idris Bin Ismail. Soil moisture detection using electrical capacitance tomography (ECT) sensor. In *Imaging Systems and Techniques (IST), 2011 IEEE International Conference on*, pages 83–88. IEEE, 2011.

[15] Ville Rimpiläinen, Lasse M. Heikkinen, and Marko Vauhkonen. Moisture distribution and hydrodynamics of wet granules during fluidized-bed drying characterized with volumetric electrical capacitance tomography. *Chemical Engineering Science*, 75:220 – 234, 2012.

[16] D Watzenig and C Fox. A review of statistical modelling and inference for electrical capacitance tomography. *Measurement Science and Technology*, 20(5):052002, 2009.

[17] W Q Yang and Lihui Peng. Image reconstruction algorithms for electrical capacitance tomography. *Measurement Science and Technology*, 14(1):R1, 2003.

[18] J. P. Kaipio and E. Somersalo. *Statistical and Computational Inverse Problems*. Springer, 2 edition, 2005.

[19] Antti Lipponen, Aku Seppänen, and Jari Kaipio. Electrical impedance tomography imaging with reduced-order model based on proper orthogonal decomposition. *Journal of Electronic Imaging*, 22(2):023008, 2013.

[20] Antti Voss, Mohammad Pour-Ghaz, Marko Vauhkonen, and Aku Seppänen. Electrical capacitance tomography to monitor unsaturated moisture ingress in cement-based materials. *Cement and Concrete Research*,

Submitted.

[21] *Process Tomography Ltd, Electrical Capacitance Tomography System Type PTL300 Instruction Manual. Software 2.3, Issue 5, 1999, http://www.tomography.com/support.htm*.

[22] Fei Wang, Qussai Marashdeh, Liang-Shih Fan, and Warsito Warsito. Electrical capacitance volume tomography: Design and applications. *Sensors*, 10(3):1890–1917, 2010.

[23] Shangjie Ren, Feng Dong, Yaoyuan Xu, and Chao Tan. Reconstruction of the three-dimensional inclusion shapes using electrical capacitance tomography. *Measurement Science and Technology*, 25(2):025403, 2014.